Journal of Membrane Science Letters 2 (2022) 100036

Contents lists available at ScienceDirect

Journal of Membrane Science Letters

journal homepage: www.elsevier.com/locate/memlet

Porous substrate affects fouling propensity of thin-film composite nanofiltration membranes

Chenyue Wu, Li Long, Zhe Yang*, Chuyang Y. Tang*

Department of Civil Engineering, the University of Hong Kong, Pokfulam, Hong Kong SAR, PR China

ARTICLE INFO

Keywords:
Nanofiltrtion memrbane
Polyamide film
Funnel effect
Localized flux
Fouling

ABSTRACT

Fouling is a critical consideration for the design of thin-film composite (TFC) nanofiltration membranes. Traditional wisdom believes that fouling propensity is primarily dictated by membrane surface properties while porous substrates play little role (on the basis on the latter have no effect on the foulant-membrane interaction). Nevertheless, porous substrates can regulate the water transport pathways, resulting in uneven water flux distribution over the membrane surface. For the first time, we experimentally investigated the micro-scale water flux distribution for nanofiltration membranes with different substrate porosities and the impact of such flux distribution pattern on fouling. With gold nanoparticles as tracers, we demonstrated more evenly distributed water flux at increasing substrate porosity. This was found to effectively alleviate membrane fouling by eliminating localized hot spots of high flux. Furthermore, higher substrate porosity also effectively enhanced the membrane water permeance due to the optimized water transport pathways. Our study reveals the fundamental relationship between the micro-scale transport behavior and the membrane fouling propensity, which provides a firm basis for the rational design of TFC membranes toward better separation performance.

1. Introduction

Nanofiltration (NF) has been widely applied in wastewater reuse, water treatment and desalination pretreatment (Kaya et al., 2015; Liu et al., 2015; Boo et al., 2018; Tang et al., 2018; Wang et al., 2020; Zhao et al., 2022). Modern NF membranes often adopt a thin-film composite (TFC) structure, with a polyamide rejection layer supported by a porous ultrafiltration substrate (Yang et al., 2018). Although NF membranes generally exhibit excellent selectivity and permeance (Guo et al., 2021; Lu and Elimelech, 2021; Yang et al., 2021; Guo et al., 2022), fouling poses a critical challenge in practical applications. Severe fouling could detrimentally impact the system efficiency, decrease membrane lifespan, increase energy consumption, and increase membrane maintenance costs (Liu et al., 2017; Goh et al., 2018; Son et al., 2018).

In general, membrane fouling is largely dictated by the interplay between foulant-membrane interaction and hydrodynamic conditions (Field et al., 1995; Liu et al., 2017; Liu et al., 2020). For example, high water flux tends to promote fouling due to more severe concentration polarization and greater drag towards the membrane surface (Wang and Tang, 2011a; Li et al., 2019; Liu et al., 2020). Meanwhile, more repulsive foulant-membrane interactions are beneficial to prevent fouling deposition and thus minimize membrane fouling. For this reason, numerous studies have focused on improving membrane surface properties such as hydrophilicity (Wu et al., 2015; Ren et al., 2020) and charge (Pan et al., 2017; Cao et al., 2021) for fouling mitigation. On the other hand, conventional wisdom often neglects the role of porous substrates on membrane fouling, on the basis that substrates do not directly affect foulant-membrane interaction.

Recent literature highlights the impact of substrates on membrane separation performance (Peng et al., 2020; Peng et al., 2022). Typical substrates of TFC NF membranes have relatively low surface porosity (e.g., ~ or <10%) (Ramon et al., 2012; Song et al., 2020), which imposes important geometric constraints for water pathways (Fig. 1A). Water molecules directly above a pore-spanning polyamide region can pass through the rejection layer in a nearly normal (vertical) direction. In contrast, water molecules far from the pore experience longer pathways as a result of the additional transverse (horizontal) distance that they have to travel before reaching the pore region (Lonsdale et al., 1971; Wijmans and Hao, 2015; Peng et al., 2022). This difference in water transport pathways leads to an uneven water flux distribution on the membrane surface, with localized high-flux hot spots over the least-hydraulic-resistance regions (i.e., the pore-spanning polyamide regions) (Ramon et al., 2012). The critical dependence of membrane fouling on (localized) water flux prompts us to hypothesize that a more porous substrate could alleviate membrane fouling by providing a more uniform flux distribution over the membrane surface (Fig. 1B).

In this study, we systematically examined the effect of porous substrate on fouling propensity of TFC NF membranes. Identical rejection

* Corresponding authors.
E-mail addresses: zheyang@connect.hku.hk (Z. Yang), tangc@hku.hk (C.Y. Tang).

https://doi.org/10.1016/j.memlet.2022.100036
Received 6 October 2022; Received in revised form 1 November 2022; Accepted 2 November 2022

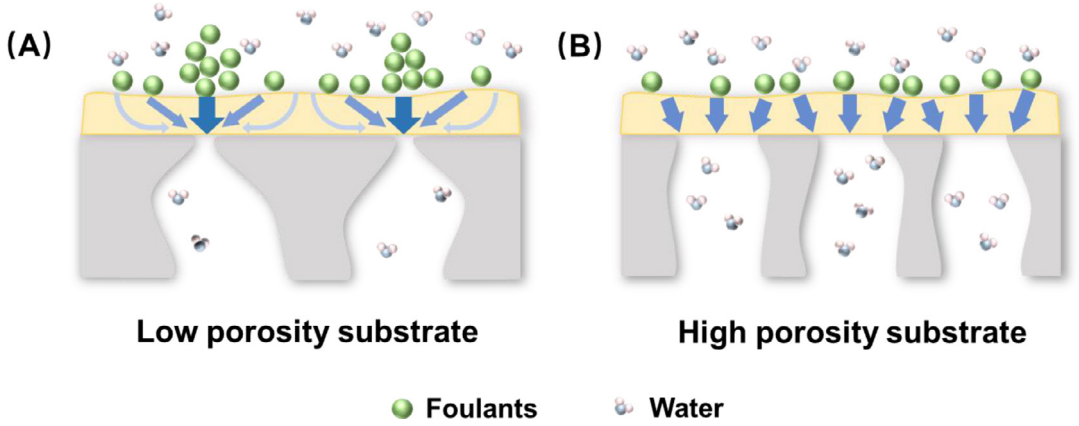

Fig. 1. Schematic illustration of fouling of (A) a TFC membrane with low-porosity substrate and (B) a TFC membrane with high-porosity substrate. Low porosity substrate causes severe funnel effect, resulting in increased water transport pathways (indicated by the length of the arrows) and an uneven flux distribution over the membrane surface (indicated by the width of the arrows). This uneven flux distribution promotes foulants accumulation at "hot spots" of high local flux. In contrast, high porosity substrate provides more uniform flux distribution over the membrane surface by allowing water to transport through the rejection layer closer to the normal direction.

layers were prepared by interfacial polymerization at a free-interface (Jiang et al., 2020) and were loaded onto substrates of difference porosities. This approach enables us to attribute the different fouling behaviors solely to the substrate properties. Using the gold nanoparticle (AuNPs) as tracers (Pacheco et al., 2010; Tan et al., 2018; Long et al., 2022), we demonstrate improved uniformity of water flux distribution for more porous substrates, which effectively mitigates membrane fouling. The mechanistic insight from this work has important implications to the design of porous substrates and fouling control of TFC NF membranes.

2. Materials and methods

2.1. Materials and chemicals

Unless otherwise specified, all chemicals were of ACS reagent grades and all solutions were prepared by deionized (DI) water produced from Milli-Q system with a resistivity of 18.2 Mohm-cm (Millipore, Billerica, MA). Three commercial polyethersulfone (PES) ultrafiltration (UF) substrates with different molecular weight cutoffs (MWCOs) were purchased from Microdyn Nadir, Germany (UP005, MWCO = 5000; UP020, MWCO = 20,000; and UP150, MWCO = 150,000). Piperazine (PIP, 99%, Sigma-Aldrich), 1,3,5-Benzenetricarbonyl trichloride (TMC, 98%, Sigma-Aldrich), and n-hexane (>95%, Fisher Chemical, UK) were used to synthesize polyamide rejection layers via interfacial polymerization (IP). Sodium chloride (NaCl) and sodium sulfate (Na_2SO_4) were all purchased from Dieckmann (China) for salt rejection tests. Bovine serum albumin (BSA, Sigma-Aldrich) was used as a model organic foulant to assess the antifouling performance. The ionic compositions of the feed solution were adjusted by the addition of NaCl and calcium chloride ($CaCl_2$, Dieckmann, China). Gold nanoparticles (AuNPs, 5 nm in diameter, BBI Solution, U. K.) was applied as tracers for investigating flux distribution over membrane surfaces. Dimethylformamide (DMF, 98 %, Sigma-Aldrich) was used to dissolve PES substrate to separate polyamide layer.

2.2. Preparation of polyamide nanofilms and NF membranes

To exclude the effect of membrane surface properties on fouling, identical polyamide rejection layers were prepared in this study by performing IP reaction at a support-free interface (Fig. S1, Supporting Information) (Choi et al., 2017; Jiang et al., 2018). A 20 mL aqueous solution of 0.02 wt.% PIP and a 10 mL hexane solution containing 0.1 wt.% TMC were used to synthesize the polyamide layer at the aqueous-organic interface for 2 min. Subsequently, the generated polyamide nanofilm at the free interface was transferred onto a PES substrate by vacuum filtration to remove excess PIP solution. The excess TMC solution was then removed, and the n-hexane solution was used to rinse the membrane surface to terminate the IP reaction. The fabricated NF membrane that consisted of a rejection layer and a substrate was denoted as NF-x, where x represents the MWCO of the substrate. According to the literature (Choi et al., 2017; Jiang et al., 2018; Long et al., 2022), NF membranes synthesized by free-interface approach are stable to withstand the cross-flow filtration.

2.3. Membrane characterization

Scanning electron microscopy (SEM, Hitachi S4800 FEG SEM) was used to observe the morphology of NF membranes. Image-Pro Plus (Media Cybernetics, Inc.) was applied to measure the pore size and porosity based on the obtained SEM images (detailed information can be found in Fig. S2, Supporting Information). To measure the thickness of the polyamide layers, the free-standing polyamide layers were transferred onto silicon wafers for atomic force microscopy characterization (AFM, Bruker, Billerica, MA). The thickness of the rejection layers ware demonstrated by the height differences between polyamide layers and silicon wafers. Fourier transform infrared (FTIR) spectroscopy (Thermo Fisher Scientific) was used to characterize the surface functional groups of NF-x membranes. Elemental compositions of membrane surface were examined by X-ray photoelectron spectroscopy (XPS, Thermo Kalpha), and the cross-linking degree was calculate based on O/N ratio (Yang et al., 2019). Water contact angle (WCA) was measured by Attension Theta Goniometer (Biolin Scientific) to determine the hydrophilicity, with the data recorded after the water droplet of 3 μL contacting the membrane surface for 5 s. Transmission electron microscopy (TEM, Philips CM100, Germany) was used out to observe the AuNPs distribution on membrane surface.

2.4. Filtration tests of gold nanoparticles

To examine membrane water flux distribution, AuNPs tracer tests were performed (Pacheco et al., 2010; Tan et al., 2018; Long et al., 2022). Prior to the test, all membranes were pre-compacted overnight with DI water at a hydraulic pressure of 5 bar in a dead-end filtration system. Subsequently, a 100 mL solution of AuNPs (5×10^{12} particles·mL^{-1}) was filtered until 15 mL of permeate solution was collected. Membranes with AuNPs on the top surface were then taken out and dried in air at room temperature for 24 h. To examine the AuNPs distribution on a membrane, its non-woven backing was carefully peeled off, and the polyamide layer was isolated by dissolving the PES substrate

using DMF according to our previous study (Long et al., 2022). The isolated polyamide film was then transferred onto a copper grid for further TEM characterization. To analyze the distribution of AuNPs, each TEM micrograph was divided in to 25 equal-area parts (5 × 5) and the surface coverage by AuNPs in each part was determined (see details in Supporting Information S5). The average surface coverage and the standard deviation were calculated. Furthermore, the coefficient of variation (CV) was used to indicate the uniformity of AuNPs distribution (Wang et al., 2022):

$$CV = \frac{std\ (coverage)}{average\ (coverage)} \tag{1}$$

2.5. Filtration tests

A cross-flow filtration setup was applied to test water flux (J_w) and salt rejection (R) under a hydraulic pressure of 5 bar at room temperature (approximately 25 °C). For each test, a new membrane coupon was installed in the cross-flow test cell and pre-compacted for 1 h using DI water under the same pressure. The pure water flux (J_w) was calculated by measuring the volume of permeate over a specified time interval based on Eq. (1):

$$J_w = \frac{\Delta V}{\Delta t \times S} \tag{2}$$

where J_w (L m^{-2} h^{-1}) is the pure water flux, V (L) is the volume of permeate, Δt (h) is the testing time, and S (m^2) is the effective membrane area. The pure water permeance (A) can be determined by the following equation:

$$A = \frac{J_w}{\Delta P} \tag{3}$$

where A (L m^{-2} h^{-1} bar^{-1}) is the pure water permeance and ΔP (bar) is the applied hydraulic pressure.

The salt rejection of fabricated membranes was tested using a feed solution containing single salt (1000 ppm NaCl or Na_2SO_4) at 5 bar. Salt rejection was calculated by the conductivity measurements of the feed and permeate solutions (Ultrameter II, Myron L) according to Eq. (3):

$$R = \frac{C_f - C_p}{C_f} \times\ 100\% \tag{4}$$

where R (%) is the salt rejection, C_p (μS/cm) is the permeate solution conductivity and C_f (μS/cm) is the feed solution conductivity.

2.6. Fouling tests

To evaluate membrane fouling propensity, BSA was used to as a model foulant (Long et al., 2022). Prior to each fouling test, a new membrane coupon was compacted overnight to achieve stable flux. The applied pressure was adjusted such that the initial flux was approximately 30 L m^{-2} h^{-1}. To initiate membrane fouling, 200 ppm BSA with 1 mM NaCl and 0.5 mM $CaCl_2$ was introduced to the feed solution. Fouling

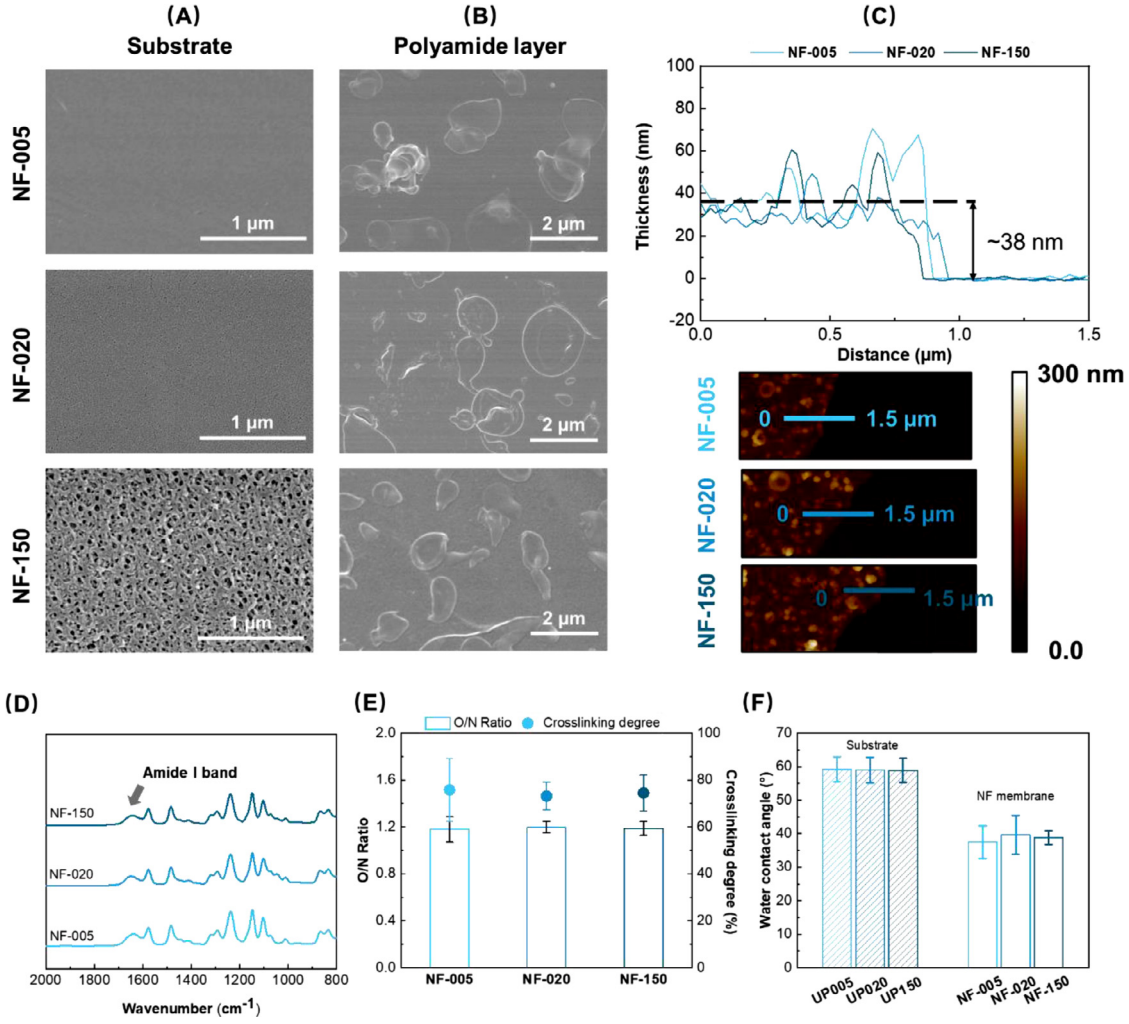

Fig. 2. Membrane characterization results: SEM images of (A) the substrates and (B) the NF membranes; (C) AFM thickness measurements of the polyamide rejection layers; (D) FTIR spectra of the NF membranes; (E) O/N ratios and cross-linking degrees of the NF membranes; (F) WCA results of the substrates and the NF membranes.

was continued for approximately 8 h, during which the water flux was measured at predetermined time intervals.

3. Results and discussion

3.1. Properties of substrates and NF membranes

Fig. 2A presents SEM images of the PES substrates. The UP005, UP020, and UP150 substrates had surface porosity values of approximately 3.3 ± 0.8%, 10.8 ± 2.7%, and 21.5 ± 0.9%, respectively (Fig. S3, Supporting Information). Their pure water permeance were 51 ± 9.9, 120.6 ± 30.9, and 837.0 ± 135.7 L m^{-2} h^{-1} bar^{-1}, respectively (Fig. S4, Supporting Information). After transferring the polyamide layers on the substrates, the corresponding fabricated NF membranes (NF-005, NF-020, and NF-150) had similar surface morphology (Fig. 2B). Additional AFM characterization revealed that all polyamide rejection layers had a comparable thickness of approximately 38 nm (Fig. 2C). The NF membranes also show similar the FTIR spectra, with the Amide I band (~1624 cm^{-1}) characteristic to the polyamide chemistry (Fig. 2D) (Tang et al., 2009). Furthermore, the cross-linking degree (Fig. 2E) and WCA results (Fig. 2F) were nearly the same. The characterization results verified that all membranes possessed identical polyamide layers despite their various substrates.

3.2. AuNPs tracer tests

While current literature appears to largely focus on the effect of macro-scale water flux on membrane fouling (Seidel and Elimelech, 2002; Wang and Tang, 2011b; Mohammad et al., 2015), the impact of micro-scale water flux distribution is often overlooked. In this study, we used AuNPs to investigate the influence of micro-scale flux on foulant deposition behavior. The micrograph of NF-150 shows relatively uniform distribution of AuNPs (Fig. 3). In contrast, large numbers of AuNPs appeared in patches over the surface of NF-005. Further statistical analysis shows the NF-005, supported on the least porous substrate, had the highest surface coverage (9.9%) by AuNPs along with the greatest standard deviation and coefficient of variation, confirming a less unform flux distribution for this membrane. According to the literature, AuNPs have been widely used as tracers for flux distribution over a membrane surface (Pacheco et al., 2010; Dai et al., 2020; Long et al., 2022), where hot spots of high local flux are accompanied with more AuNP accumulation (Tan et al., 2018). Thus, the patch-like deposition of AuNPs over NF-005 implies a highly non-uniform flux distribution for this membrane. In general, water molecules converging from the membrane surface to a substrate pore when passing through the polyamide layer (Fig. 1). This funnel effect results in hot spots of high flux over the pore-spanning polyamide regions. Since NF-005 had the least porous substrate, it would suffer the most severe funnel

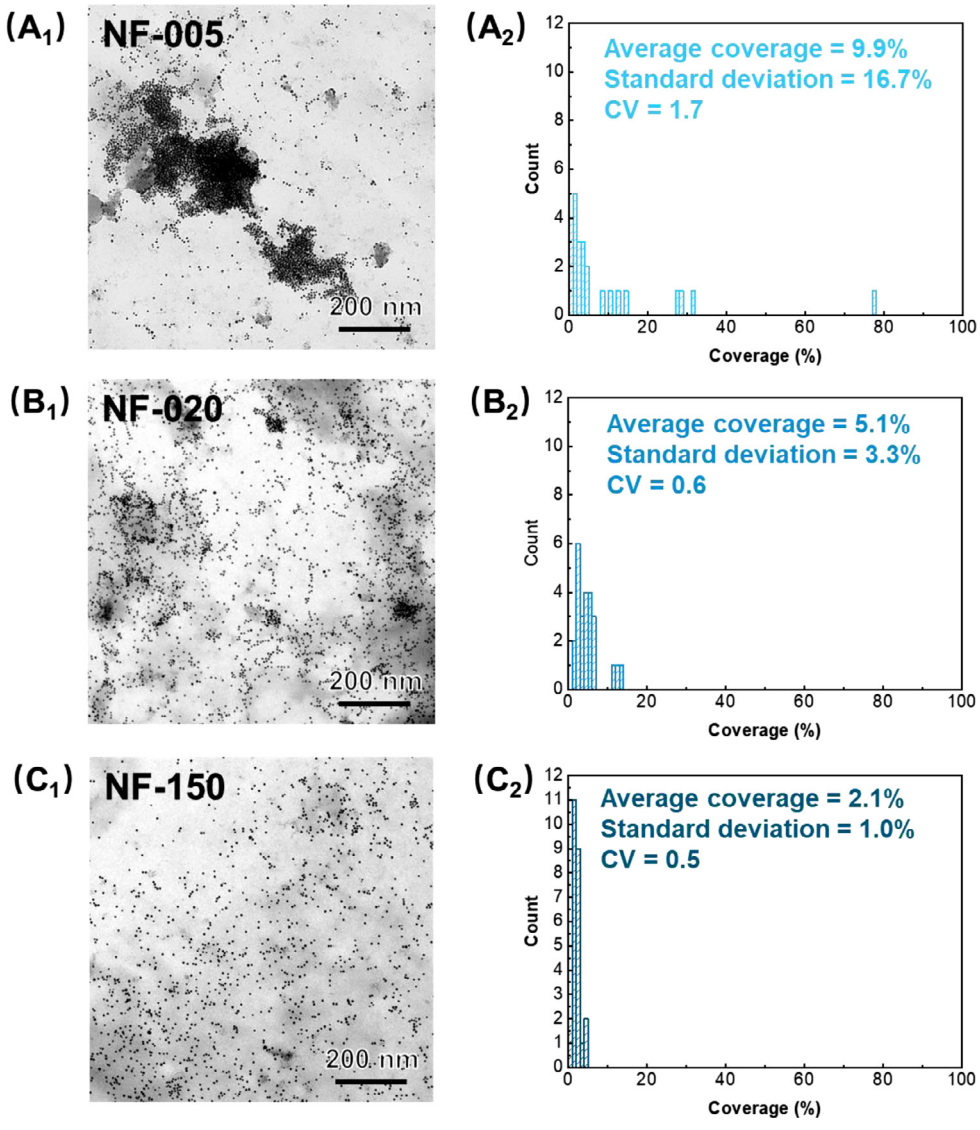

Fig. 3. TEM plan images and analysis of AuNP distribution for (A) NF-005, (B) NF-020 and (C) NF-150. To analyze the AuNP distribution, each TEM micrograph was divided into 25 equal-area parts. The surface coverage by AuNPs in each part was determined by image analysis, and their distributions are presented. The detailed procedures can be found in Supporting Information S5.

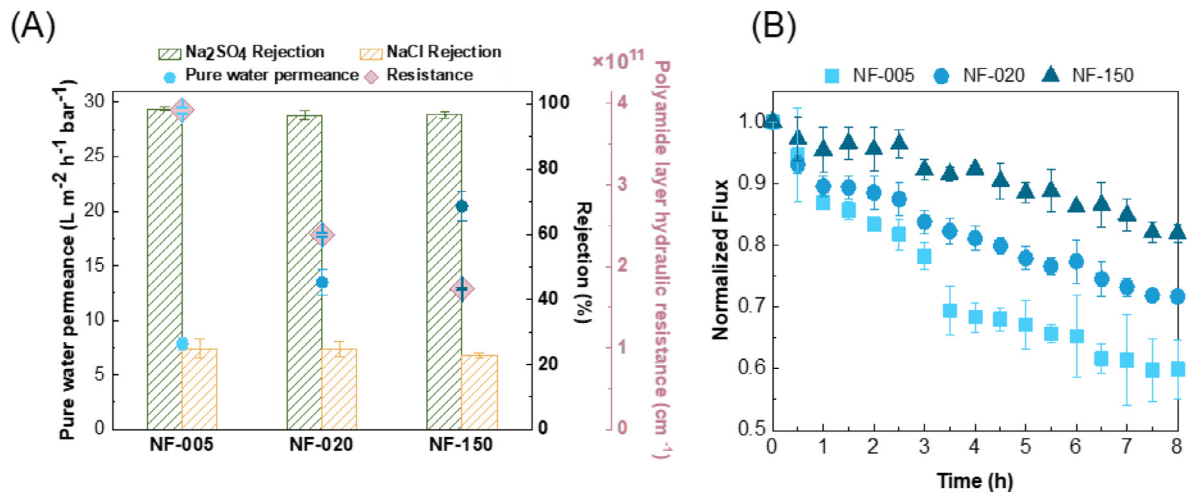

Fig. 4. (A) Separation performance. (B) Fouling test results for NF-005, NF-020, and NF-150. The separation performance was evaluated by a cross-flow set-up for at least three replicates of each membrane. Salt rejection was tested by 1000 ppm solution with single type of salt (NaCl and Na_2SO_4). Hydraulic resistance of polyamide layer was calculated in Section S4 (Supporting Information). Fouling tests were conducted in duplicates for each membrane type. An identical initial water flux of 30 L m^{-2} h^{-1} was used by adjusting the hydraulic pressure. The error bars are based on the range of the two replicates.

effect (Fig. 3A), which explains its highly non-uniform pattern of AuNP deposition. The reduced uniformity in flux distribution for less porous substrates agrees well with a recent modelling work (Wang et al., 2022). Such a critical effect of substrate porosity on local flux distribution may translate into major influence on membrane fouling propensity (see Section "antifouling performance").

3.3. Separation and antifouling performance

3.3.1. Separation performance

Fig. 4A shows similar rejections of Na_2SO_4 (~96–98%) and NaCl (~25%) for all the membranes which is attributed to the use of identical rejection layers (Fig. 2). However, increasing substrate porosity from 3.3 ± 0.8% (NF-005) to 21.5 ± 0.9% (NF-150) nearly tripled the pure water permeance. This greatly improved water permeance is consistent with the mitigated funnel effect for the more porous substrate. Indeed, further analysis (Section S4, Supporting Information) suggests that the hydraulic resistance of the polyamide layer in NF-150 membrane (1.8×10^{11} cm^{-1}) is less than half of that of NF-005 membrane (4.4×10^{11} cm^{-1}) (Fig. 4A), despite the use of identical polyamide layers in these membranes. The greatly increased hydraulic resistance of the polyamide layer in NF-005 can be explained by the increased water transport pathlength in this membrane due to the low-porosity substrate (Fig. 1A). According to a recent modeling work (Wang et al., 2022), lengthened water transport path due to severe funnel effect could potentially reduce water permeation efficiency by an order of magnitude.

3.3.2. Antifouling performance

We performed membrane fouling tests using BSA as a model foulant. An identical initial flux of 30 L m^{-2} h^{-1} was applied to ensure a fair comparison. As shown in Fig. 4B, the water flux decreased by almost 40% for NF-005 after the 8-h fouling test. In contrast, NF-150 experienced a more moderate water flux decline of approximately 20%, which confirms our hypothesis that increasing substrate porosity results in enhanced antifouling performance. Even though the use of the same initial flux ensures identical average macro-scale fluxes in all cases, the membranes would experience different localized water flux at the micro-scale. Increasing substrate porosity optimizes the water transport pathways and result in more uniform flux distribution (Fig. 1). The mitigated funnel effect minimizes the presence of hot spots of high flux (Fig. 3), which explains the improved fouling performance.

4. Conclusion

Traditional anti-fouling membrane design often solely emphasize the importance of membrane surface properties. For the first time, this study experimentally demonstrated the role of substrate porosity on membrane fouling propensity. The porous substrate can influence the water transport path, which regulates the localized flux distribution over the membrane surface. Low-porosity substrates may result in severe funnel effect, whose high-flux hot spots are more vulnerable to foulant deposition. Improving substrate porosity can greatly alleviate such unfavorable effect, providing greatly improved antifouling performance. The work presented in this study reveals the fundamental relationship between the micro-scale transport behavior and the membrane fouling propensity, which enables a rational design of TFC membrane substrate toward better antifouling performance. Future studies need to further systematically evaluate the mechanical strength of such anti-fouling membranes.

Data availability

Data will be made available on request.

Declaration of Comepting Interest

The authors declare no conflict of interest.

CRediT authorship contribution statement

Chenyue Wu: Methodology, Investigation, Writing – original draft. **Li Long:** Methodology, Visualization. **Zhe Yang:** Conceptualization, Methodology, Writing – review & editing. **Chuyang Y. Tang:** Conceptualization, Methodology, Supervision, Writing – review & editing.

Acknowledgments

We also acknowledge the full support by a grant from the General Research Fund (Project # 17201921) of the Research Grants Council of Hong Kong.

Supplementary materials

Supplementary material associated with this article can be found, in the online version, at doi:10.1016/j.memlet.2022.100036.

References

Boo, C., Wang, Y., Zucker, I., Choo, Y., Osuji, C.O., Elimelech, M., 2018. High performance nanofiltration membrane for effective removal of perfluoroalkyl substances at high water recovery. Environ. Sci. Technol. 52, 7279–7288. doi:10.1021/acs.est.8b01040.

Cao, X.-L., Zhou, F.-Y., Cai, J., Zhao, Y., Liu, M.-L., Xu, L., Sun, S.-P., 2021. High-permeability and anti-fouling nanofiltration membranes decorated by asymmetric organic phosphate. J. Membr. Sci. 617. doi:10.1016/j.memsci.2020.118667.

Choi, W., Jeon, S., Kwon, S.J., Park, H., Park, Y.-I., Nam, S.-E., Lee, P.S., Lee, J.S., Choi, J., Hong, S., Chan, E.P., Lee, J.-H., 2017. Thin film composite reverse osmosis membranes prepared via layered interfacial polymerization. J. Membr. Sci. 527, 121–128. doi:10.1016/j.memsci.2016.12.066.

Dai, R., Wang, X., Tang, C.Y., Wang, Z., 2020. Dually charged MOF-based thin-film nanocomposite nanofiltration membrane for enhanced removal of charged pharmaceutically active compounds. Environ. Sci. Technol. 54, 7619–7628. doi:10.1021/acs.est.0c00832.

Field, R.W., Wu, D., Howell, J.A., Gupta, B.B., 1995. Critical flux concept for microfiltration fouling. J. Membr. Sci. 100, 259–272. doi:10.1016/0376-7388(94)00265-Z.

Goh, P.S., Lau, W.J., Othman, M.H.D., Ismail, A.F., 2018. Membrane fouling in desalination and its mitigation strategies. Desalination 425, 130–155. doi:10.1016/j.desal.2017.10.018.

Guo, H., Dai, R., Xie, M., Peng, L.E., Yao, Z., Yang, Z., Nghiem, L.D., Snyder, S.A., Wang, Z., Tang, C.Y., 2022. Tweak in puzzle: tailoring membrane chemistry and structure toward targeted removal of organic micropollutants for water reuse. Environ. Sci. Technol. Lett. doi:10.1021/acs.estlett.2c00094.

Guo, H., Li, X., Yang, W., Yao, Z., Mei, Y., Peng, L.E., Yang, Z., Shao, S., Tang, C.Y., 2021. Nanofiltration for drinking water treatment: a review. Front. Chem. Sci. Eng. 1–18. doi:10.1007/s11705-021-2103-5.

Jiang, C., Zhang, L., Li, P., Sun, H., Hou, Y., Niu, Q.J., 2020. Ultrathin film composite membranes fabricated by novel *in situ* free interfacial polymerization for desalination. ACS Appl. Mater. Interfaces 12, 25304–25315. doi:10.1021/acsami.0c05166.

Jiang, Z., Karan, S., Livingston, A.G., 2018. Water transport through ultrathin polyamide nanofilms used for reverse osmosis. Adv. Mater. 30, 1705973. doi:10.1002/adma.201705973.

Kaya, C., Sert, G., Kabay, N., Arda, M., Yüksel, M., Egemen, Ö., 2015. Pre-treatment with nanofiltration (NF) in seawater desalination—preliminary integrated membrane tests in Urla, Turkey. Desalination 369, 10–17. doi:10.1016/j.desal.2015.04.029.

Li, W., Su, X., Palazzolo, A., Ahmed, S., 2019. Numerical modeling of concentration polarization and inorganic fouling growth in the pressure-driven membrane filtration process. J. Membr. Sci. 569, 71–82. doi:10.1016/j.memsci.2018.10.007.

Liu, C., Lee, J., Ma, J., Elimelech, M., 2017. Antifouling thin-film composite membranes by controlled architecture of zwitterionic polymer brush layer. Environ. Sci. Technol. 51, 2161–2169. doi:10.1021/acs.est.6b05992.

Liu, J., Huang, T., Ji, R., Wang, Z., Tang, C.Y., Leckie, J.O., 2020. Stochastic collision-attachment-based Monte Carlo simulation of colloidal fouling: transition from foulant-clean-membrane interaction to foulant-fouled-membrane interaction. Environ. Sci. Technol. 54, 12703–12712. doi:10.1021/acs.est.0c04165.

Liu, T.-Y., Liu, Z.-H., Zhang, R.-X., Wang, Y., Van der Bruggen, B., Wang, X.-L., 2015. Fabrication of a thin film nanocomposite hollow fiber nanofiltration membrane for wastewater treatment. J. Membr. Sci. 488, 92–102. doi:10.1016/j.memsci.2015.04.020.

Long, L., Wu, C., Yang, Z., Tang, C.Y., 2022. Carbon nanotube interlayer enhances water permeance and antifouling performance of nanofiltration membranes: mechanisms and experimental evidence. Environ. Sci. Technol. 56, 2656–2664. doi:10.1021/acs.est.1c07332.

Lonsdale, H.K., Riley, R.L., Lyons, C.R., Carosella, D.P., 1971. Transport in composite reverse osmosis membranes. In: Membrane Processes in Industry and Biomedicine. Springer, pp. 101–122.

Lu, X., Elimelech, M., 2021. Fabrication of desalination membranes by interfacial polymerization: history, current efforts, and future directions. Chem. Soc. Rev. 50, 6290–6307. doi:10.1039/d0cs00502a.

Mohammad, A.W., Teow, Y.H., Ang, W.L., Chung, Y.T., Oatley-Radcliffe, D.L., Hilal, N., 2015. Nanofiltration membranes review: recent advances and future prospects. Desalination 356, 226–254. doi:10.1016/j.desal.2014.10.043.

Pacheco, F.A., Pinnau, I., Reinhard, M., Leckie, J.O., 2010. Characterization of isolated polyamide thin films of RO and NF membranes using novel TEM techniques. J. Membr. Sci. 358, 51–59. doi:10.1016/j.memsci.2010.04.032.

Pan, Y., Xu, R., Lü, Z., Yu, S., Liu, M., Gao, C., 2017. Enhanced both perm-selectivity and fouling resistance of poly(piperazine-amide) nanofiltration membrane by incorporating sericin as a co-reactant of aqueous phase. J. Membr. Sci. 523, 282–290. doi:10.1016/j.memsci.2016.10.011.

Peng, L.E., Yang, Z., Long, L., Zhou, S., Guo, H., Tang, C.Y., 2022. A critical review on porous substrates of TFC polyamide membranes: mechanisms, membrane performances, and future perspectives. J. Membr. Sci. 641, 119871. doi:10.1016/j.memsci.2021.119871.

Peng, L.E., Yao, Z., Yang, Z., Guo, H., Tang, C.Y., 2020. Dissecting the role of substrate on the morphology and separation properties of thin film composite polyamide membranes: seeing is believing. Environ. Sci. Technol. 54, 6978–6986. doi:10.1021/acs.est.0c01427.

Ramon, G.Z., Wong, M.C.Y., Hoek, E.M.V., 2012. Transport through composite membrane, part 1: is there an optimal support membrane? J. Membr. Sci. 415-416, 298–305. doi:10.1016/j.memsci.2012.05.013.

Ren, L., Chen, J., Lu, Q., Wang, C., Han, J., Huang, K., Pan, X., Wu, H., 2020. Construction of high selectivity and antifouling nanofiltration membrane via incorporating macrocyclic molecules into active layer. J. Membr. Sci. 597. doi:10.1016/j.memsci.2019.117641.

Seidel, A., Elimelech, M., 2002. Coupling between chemical and physical interactions in natural organic matter (NOM) fouling of nanofiltration membranes: implications for fouling control. J. Membr. Sci. 203, 245–255. doi:10.1016/S0376-7388(02)00013-3.

Son, M., Yang, W., Bucs, S.S., Nava-Ocampo, M.F., Vrouwenvelder, J.S., Logan, B.E., 2018. Polyelectrolyte-based sacrificial protective layer for fouling control in reverse osmosis desalination. Environ. Sci. Technol. Lett. 5, 584–590. doi:10.1021/acs.estlett.8b00400.

Song, X., Gan, B., Qi, S., Guo, H., Tang, C.Y., Zhou, Y., Gao, C., 2020. Intrinsic nanoscale structure of thin film composite polyamide membranes: connectivity, defects, and structure-property correlation. Environ. Sci. Technol. 54, 3559–3569. doi:10.1021/acs.est.9b05892.

Tan, Z., Chen, S., Peng, X., Zhang, L., Gao, C., 2018. Polyamide membranes with nanoscale turing structures for water purification. Science 360. doi:10.1126/science.aar630.

Tang, C.Y., Kwona, Y.-N., Leckiea, J.O., 2009. Effect of membrane chemistry and coating layer on physiochemical properties of thin film composite polyamide RO and NF membranes I. FTIR and XPS characterization of polyamide and coating layer chemistry. Desalination 242, 149–167. doi:10.1016/j.desal.2008.04.

Tang, C.Y., Yang, Z., Guo, H., Wen, J.J., Nghiem, L.D., Cornelissen, E., 2018. Potable water reuse through advanced membrane technology. Environ. Sci. Technol. 52, 10215–10223. doi:10.1021/acs.est.8b00562.

Wang, F., Yang, Z., Tang, C.Y., 2022. Modeling water transport in interlayered thin-film nanocomposite membranes: gutter effect vs funnel effect. ACS ES&T Eng. doi:10.1021/acsestengg.2c00133.

Wang, Y.N., Tang, C.Y., 2011a. Protein fouling of nanofiltration, reverse osmosis, and ultrafiltration membranes—the role of hydrodynamic conditions, solution chemistry, and membrane properties. J. Membr. Sci. 376, 275–282. doi:10.1016/j.memsci.2011.04.036.

Wang, Y., Ju, L., Xu, F., Tian, L., Jia, R., Song, W., Li, Y., Liu, B., 2020. Effect of a nanofiltration combined process on the treatment of high-hardness and micropolluted water. Environ. Res. 182, 109063. doi:10.1016/j.envres.2019.109063.

Wang, Y.N., Tang, C.Y., 2011b. Nanofiltration membrane fouling by oppositely charged macromolecules: investigation on flux behavior, foulant mass deposition, and solute rejection. Environ. Sci. Technol. 45, 8941–8947. doi:10.1021/es202709r.

Wijmans, J.G., Hao, P., 2015. Influence of the porous support on diffusion in composite membranes. J. Membr. Sci. 494, 78–85. doi:10.1016/j.memsci.2015.07.047.

Wu, J., Wang, Z., Yan, W., Wang, Y., Wang, J., Wang, S., 2015. Improving the hydrophilicity and fouling resistance of RO membranes by surface immobilization of PVP based on a metal-polyphenol precursor layer. J. Membr. Sci. 496, 58–69. doi:10.1016/j.memsci.2015.08.044.

Yang, Z., Guo, H., Yao, Z.-k., Mei, Y., Tang, C.Y., 2019. Hydrophilic silver nanoparticles induce selective nanochannels in thin film nanocomposite polyamide membranes. Environ. Sci. Technol. 53, 5301–5308. doi:10.1021/acs.est.9b00473.

Yang, Z., Long, L., Wu, C., Tang, C.Y., 2021. High permeance or high selectivity? Optimization of system-scale nanofiltration performance constrained by the upper bound. ACS ES&T Eng. doi:10.1021/acsestengg.1c00237.

Yang, Z., Ma, X.H., Tang, C.Y.Y., 2018. Recent development of novel membranes for desalination. Desalination 434, 37–59. doi:10.1016/j.desal.2017.11.046.

Zhao, Z., Feng, S., Xiao, C., Luo, J., Song, W., Wan, Y., Li, S., 2022. Exploring ions selectivity of nanofiltration membranes for rare earth wastewater treatment. Sep. Purif. Technol. 289. doi:10.1016/j.seppur.2022.120748.